JOURNAL OF GEOPHYSICAL RESEARCH, VOL. 101, NO. C7, PAGES 16,543–16,550, JULY 15, 1996

# Waves and currents over a fixed rippled bed
# 2. Bottom and apparent roughness experienced by currents in the presence of waves

Paul Peter Mathisen[1]

Department of Civil and Environmental Engineering, Worcester Polytechnic Institute
Worcester, Massachusetts

Ole Secher Madsen

Ralph M. Parsons Laboratory, Department of Civil and Environmental Engineering, Massachusetts Institute of Technology, Cambridge

**Abstract.** This paper is the second of two papers which present the results of an experimental study to verify the use of a single bottom roughness length scale to characterize wave and current boundary layer flows over a rough bed. While the first paper [*Mathisen and Madsen*, this issue] included analysis of wave attenuation measurements to estimate the bottom roughness experienced by waves in the presence and absence of a current, this paper includes the analysis of time-averaged velocity profiles to estimate the bottom and apparent roughness experienced by a current in the presence of waves. In this paper, velocity profiles predicted by the *Grant and Madsen* [1986] model are compared with measured velocity profiles. Apparent hydraulic roughness predictions of the *Grant and Madsen* [1986] model are shown to underpredict the apparent hydraulic roughnesses experienced by the current. This difference is shown to be a result of an underprediction of the wave boundary layer thickness and of a steady streaming or mass transport which is induced by the wave motion within the wave boundary layer of the combined wave-current flow. By modifying the wave boundary layer thickness and estimating the wave-induced mass transport from pure wave experiments, the bottom roughness for pure current, pure wave, and combined wave-current boundary layer flows is shown to be characterized by a single roughness scale.

## 1. Introduction

### The Apparent Hydraulic Roughness

The presence of oscillatory waves has been shown to have significant effects on the characteristics of slowly varying currents in coastal regions. Because of the short timescale associated with oscillatory wave motion, high-velocity gradients exist within the wave boundary layer which result in high turbulence intensity and impose significant shear stresses on the bottom. The high turbulence intensity and shear stresses within the wave boundary layer also increase the boundary resistance experienced by the current. Due to the increased near-bottom turbulence effects, the current velocity profile outside the wave boundary layer reflects an enhanced or apparent bottom roughness when waves are present. Verification of the existence of this enhanced roughness has been provided by experiments of *Bakker and van Doorn* [1978], *Brevik and Aas* [1980], *Kemp and Simons* [1982], and others.

A number of investigators [*Lundgren*, 1972; *Smith*, 1977; *Tanaka and Shuto*, 1981; *Christoffersen and Jonsson*, 1985; *Grant and Madsen*, 1979, 1986] have developed eddy viscosity models to characterize current velocity profiles in the presence of waves. In these eddy viscosity models the apparent roughness depends on the definitions of the vertical eddy viscosity distributions and the bottom roughness. In all cases a single bottom roughness is assumed for both waves and currents.

This paper is the second of two papers which address the use of a single bottom roughness length scale to characterize boundary layers for waves, currents, and combined wave-current flows. In the first paper [*Mathisen and Madsen*, this issue] (hereafter identified as MM1), detailed analysis of wave attenuation measurements was used to show that the roughness experienced by waves ($k_w$) may be adequately characterized using the roughness experienced by a pure current ($k_c$) when results were analyzed using the eddy viscosity model of *Grant and Madsen* [1979, 1986]. The analysis of MM1 also showed that the roughness for waves in the presence of a current ($k_{wc}$) was essentially equal to the roughness for pure waves.

### Objective

This paper includes a detailed analysis of time-averaged velocity profiles measured in the same experimental facility and setup as described in section 2 of MM1. The objective of this paper is to show that the roughnesses determined in MM1, when used in conjunction with an eddy viscosity model, can be used to determine velocity profiles for currents in the presence of waves. After a description of the procedures to determine the apparent hydraulic roughnesses in section 2 it is shown in

[1]Formerly at Ralph M. Parsons Laboratory, Massachusetts Institute of Technology, Cambridge.



Paper number 96JC00955.
0148-0227/96/96JC-00955$09.00

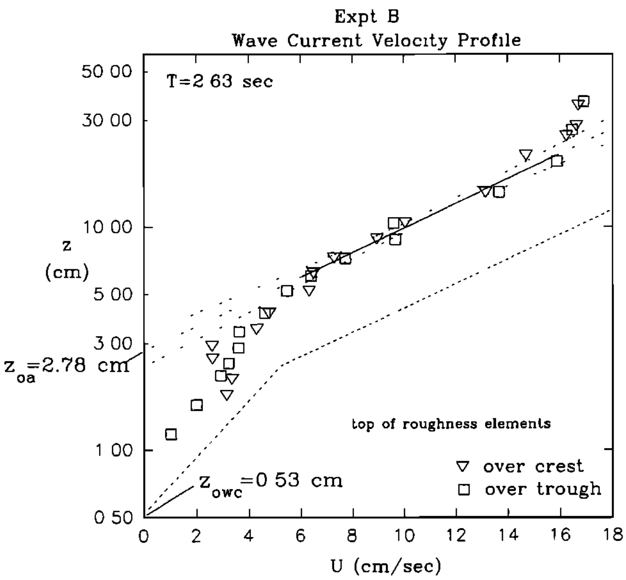


**Figure 1.** Time-averaged velocity profile for combined wave-current flow ($U$ = 16 cm/s and $T$ = 2.63 s): regression is shown as solid line in logarithmic region surrounded by 95% confidence intervals, and prediction of standard form of *Grant and Madsen*'s [1986] model (GM model) is shown as dashed line.

section 3 that velocity profiles predicted using a straight application of the *Grant and Madsen* [1986] model do not match experimentally determined velocity profiles. This discrepancy is explained partly by an enhanced wave boundary layer thickness in section 4 and partly by a wave-induced streaming within the wave boundary layer in section 5. Agreement between predicted and measured velocity profiles is obtained by modifying the *Grant and Madsen* [1986] model to account for these two effects.

## 2. Experimental Determinations of the Apparent Hydraulic Roughness

The experimental methodology in this paper is based on the analysis of time-averaged velocity profiles in order to estimate the apparent roughness experienced by a current. Procedures for obtaining time-averaged velocity profiles for combined wave-current flows were essentially the same as the procedures for pure current velocity profiles presented in MM1. For the combined wave-current flow experiments it suffices to point out that a minimum sampling duration of 12 min was needed to ensure the standard deviation of the mean current speed to be less than 0.5 cm/s. Sampling durations all exceeded the 12 min minimum and were adjusted to coincide with an integral number of wave cycles (typically, 512 cycles). Fast Fourier transforms (FFTs) yielded profiles of wave velocity amplitude and phase as well as time-averaged velocity profiles.

Measured time-averaged velocity profiles provided estimates of the apparent current roughness. The time-averaged velocity profiles (measured over a crest and trough) for a 16 cm/s current in the presence of 2.63-s periodic waves, shown in Figure 1, clearly show that a logarithmic region exists between 6 and 15 cm. The region below this logarithmic region may be considered to be within the wave boundary layer. In the wave boundary layer the velocity measurements over the crest are not equal to those over the trough, indicating that some effects of individual bed forms are present within this region (up to an elevation of approximately 5 cm). The region above 15 cm is in the free stream and is outside of the logarithmic region.

In accordance with the *Grant and Madsen* [1986] model, hereafter referred to as the GM model, the velocity profile in the logarithmic region is

$$u = (u_{*_c}/\kappa) \ln (z/z_{oa}) \tag{1}$$

where $z$ is measured from the flume bottom, $u_{*_c}$ is the current shear velocity, $\kappa$ is von Karman's constant (taken to be 0.4), and $z_{oa}$ is the apparent hydraulic roughness. The resulting fit, indicated by the solid line in Figure 1, yields a current shear velocity of $u_{*_c} = 3.15$ cm/s and an apparent hydraulic roughness of $z_{oa} = 2.78$ cm. Shear velocities and apparent hydraulic roughnesses for all experiments were obtained following this methodology and, along with additional information identifying specific experimental conditions, are listed in Table 1 (under the headings "Measured $u_{*_c}$" and "Measured $z_{oa}$"). The centered dots in Table 1 indicate experimental conditions for which no current profile measurements were made. Experimental results shown in Table 1 include 10-cm bar spacings, except for a few experiments using a 20-cm bar spacing (as noted in Table 1).

## 3. Predictions of Apparent Hydraulic Roughness

For combined wave-current flows the GM model defines the apparent hydraulic roughness as

$$z_{oa} = z_{owc}^{\varepsilon} \delta_{wc}^{1-\varepsilon} \tag{2}$$

where $z_{owc}$ is the hydraulic roughness, $\varepsilon$ is defined as $u_{*_c}/u_{*_m}$, and $\delta_{wc}$ is the wave boundary layer thickness. The hydraulic roughness $z_{owc}$ is defined to be equal to $k_{wc}/30$, in which $k_{wc}$ is the wave bottom roughness in the presence of a current. The maximum combined wave-current shear velocity $u_{*_m}$ is defined by

$$u_{*_m}^2 = u_{*_{wm}}^2 + u_{*_c}^2 \tag{3}$$

where $u_{*_{wm}}$ is the maximum wave shear velocity. Values of $k_{wc}$ and $u_{*_{wm}}$, obtained in MM1, are listed in Table 1. With $u_{*_m}$ defined by (3) the wave boundary layer thickness $\delta_{wc}$ is estimated from

$$\delta_{wc} = 2\kappa u_{*_m}/\omega \tag{4}$$

where $\omega$ is the radian frequency.

The predicted velocity profile obtained using (2) through (4) for experiment B is shown as the dashed line in Figure 1. The predicted velocity profile does not match the experimental data well. The predicted apparent hydraulic roughness is only 1.26 cm, which is much smaller than the measured apparent hydraulic roughness of 2.78 cm. Predicted apparent hydraulic roughnesses for all experiments are included in Table 1 (under the heading "Predicted $z_{oa}$, cm, $\delta$ via Standard GM Model"), from which it is seen that application of the standard form of the Grant-Madsen model greatly underpredicts the measured apparent hydraulic roughnesses in all cases, despite having chosen the upper limit of the GM model's definition of the wave boundary layer thickness.

**Table 1.** Comparisons Between Measured and Predicted Apparent Roughness Estimates

| Experiment ID | Pure Wave Experiment ID* | $T$, s | $u_{bm}$, cm/s | $u_{*wm}$, cm/s | $k_{wc}$, cm | $U$, cm/s | Measured $u_{*c}$, cm/s | Measured $z_{oa}$, cm | Predicted $z_{oa}$, cm, $\delta$ via Standard GM Model | Predicted $z_{oa}$, cm, $\delta$ Set at 6 cm | Measured $\bar{u}_w$, cm/s | Predicted $z_{oa}$, cm, With Mass Transport and $\delta = 6$ cm |
|---|---|---|---|---|---|---|---|---|---|---|---|---|
| A | a | 2.24 | 16.9 | 6.76 | 19.5 | 16 | 3.44 | 3.30 | 1.30 | 2.18 | −1.9 | 2.72 |
| B | b | 2.63 | 18.0 | 6.36 | 15.7 | 16 | 3.15 | 2.78 | 1.26 | 2.04 | −1.2 | 2.37 |
| C | c | 2.89 | 17.9 | 6.33 | 17.7 | 16 | 3.50 | 3.68 | 1.40 | 2.04 | −4.0 | 3.22 |
| G | a | 2.24 | 16.9 | 6.76 | 20.1 | 12 | ··· | ··· | ··· | ··· | −1.9 | ··· |
| H | b | 2.63 | 18.2 | 6.17 | 15.0 | 12 | 2.09 | 3.22 | 1.40 | 2.69 | −1.2 | 3.39 |
| I | c | 2.89 | 18.3 | 7.09 | 24.9 | 12 | ··· | ··· | ··· | ··· | −4.0 | ··· |
| J | d | 2.24 | 11.5 | 5.27 | 21.3 | 12 | 2.46 | 3.66 | 1.19 | 2.42 | −1.9 | 3.31 |
| K | e | 2.63 | 12.8 | 5.12 | 18.4 | 12 | 2.08 | 2.84 | 1.26 | 2.55 | −1.2 | 3.21 |
| L | f | 2.89 | 12.7 | 5.46 | 23.0 | 12 | 2.95 | 4.84 | 1.39 | 2.24 | −3.2 | 3.46 |
| M† | m | 2.24 | 17.4 | 5.50 | 11.5 | 16 | ··· | ··· | ··· | ··· | −1.0 | ··· |
| N† | n | 2.63 | 18.4 | 5.36 | 10.7 | 16 | 2.8 | 3.05 | 1.01 | 1.86 | −1.4 | 2.27 |
| O† | o | 2.89 | 18.6 | 5.58 | 12.5 | 16 | ··· | ··· | ··· | ··· | −2.5 | ··· |
| P† | m | 2.24 | 17.4 | 5.36 | 9.6 | 12 | ··· | ··· | ··· | ··· | −1.0 | ··· |
| Q† | n | 2.63 | 18.6 | 5.88 | 12.2 | 12 | 2.15 | 3.33 | 1.24 | 2.41 | −1.4 | 3.13 |
| R† | o | 2.89 | 19.0 | 6.44 | 16.2 | 12 | ··· | ··· | ··· | ··· | −2.5 | ··· |

GM model is the *Grant and Madsen* [1986] model.
*Pure wave experiments corresponding to the wave-current experiments are denoted by lowercase letters.
†Twenty-centimeter roughness spacing.

## 4. Effects of an Enhanced Boundary Layer Thickness

In part, the poor correspondence between observed and predicted apparent hydraulic roughnesses can be attributed to an enhanced boundary layer thickness resulting from the large roughness elements which were used for these experiments. The boundary layer thickness predicted by (4) is 2.54 cm, as depicted by the kink in the solid line in Figure 1. However, the measured data in Figure 1 indicate a boundary layer thickness of approximately 6 cm. The failure of the standard form of the GM model's prediction of the wave boundary layer thickness and therefore its inability to reproduce detailed wave velocity information inside the wave boundary layer of the kind shown in Figures 2a and 2b are not surprising since the large bottom roughnesses in the present experiments are far beyond this and any other wave-current model's formal limit of validity. The issue of "extrapolation" of the GM model beyond its formal limit of validity was discussed extensively in MM1 and should be kept in mind when we proceed by adopting the GM model's formulation of the characteristics of currents in the presence of waves as the basis for our data analysis.

The enhanced boundary layer thickness can also be seen in profiles of wave orbital velocity amplitude and phase. The first harmonic wave velocity amplitude for experiment B (identified in Table 1) is plotted in Figure 2a. Above 6 cm the amplitude of the wave velocity follows a trend similar to that predicted by inviscid linear theory. Below 4 cm the velocity amplitude measurements over the crest are higher than those over the trough. The differences between the wave velocity amplitudes for the crest and trough below 4 cm result from the effects of individual roughness elements. The overshoot effect evident in Figure 2a for the interval of $z$ from 3 to 6 cm is characteristic of oscillatory boundary layers and suggests that the wave boundary layer extends to an elevation of approximately 6 cm above the bottom. This effect is also apparent in the phase profile for the first harmonic wave velocity amplitude, which is plotted in Figure 2b. As can be seen in Figure 2b, the profile is affected by the turbulent shear stresses below 6 or 7 cm. Thus the thickness of the wave boundary layer predicted by the standard Grant-Madsen model is considerably lower than the actual boundary layer thickness in these experiments. This enhanced boundary layer thickness is also apparent in the wave orbital velocity amplitude and phase profiles for pure waves [*Mathisen*, 1993; *Mathisen and Madsen*, 1993].

The enhanced boundary layer thickness is likely a result of the large roughness elements used for these experiments. The height of the triangular bars, $\eta = 1.5$ cm, was necessary to ensure a reasonable simulation of a naturally rippled bottom for the given wave conditions. Since the same enhanced boundary layer thickness of 6 cm was characteristic of all experiments using this bottom configuration (including the wide spacing

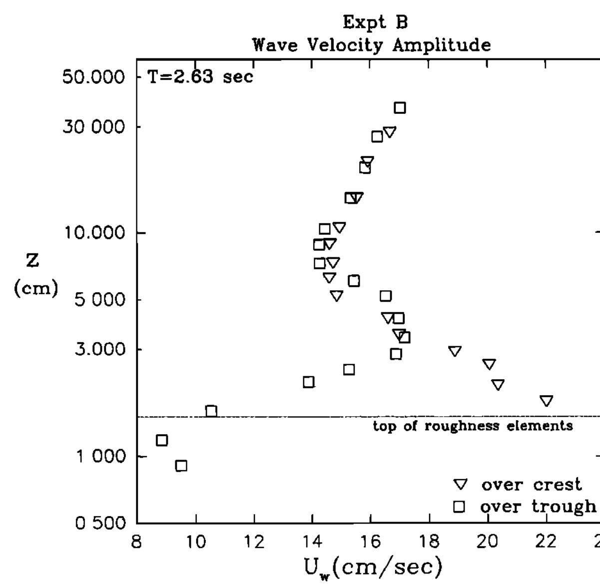


**Figure 2a.** Profile of first harmonic wave velocity amplitude for combined wave-current flow ($U$ = 16 cm/s and $T$ = 2.63 s).

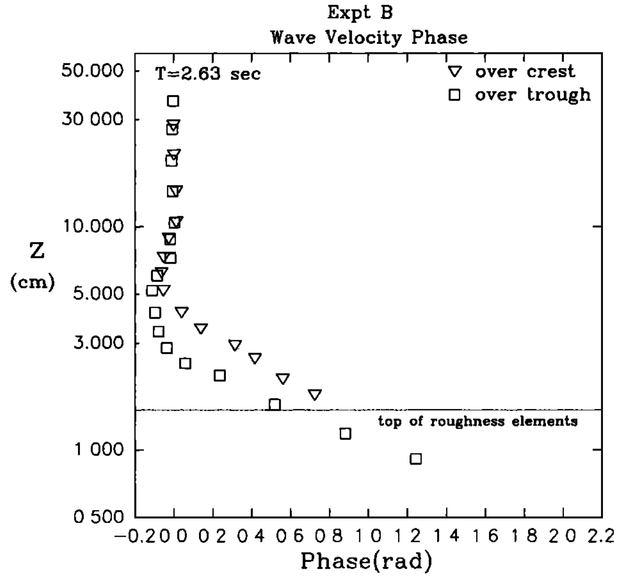


**Figure 2b.** Profile of first harmonic wave velocity phase for combined wave-current flow ($U$ = 16 cm/s and $T$ = 2.63 s).

experiments), the height of the boundary layer appears to be scaled by the height of the roughness elements, i.e., $\delta_{wc} \cong 4\eta$ for these particular roughness elements.

The predicted current velocity profile for experiment B from the GM model with $\delta_{wc} \approx 4\eta = 6$ cm replacing the original definition given by (4) is shown in Figure 3. The apparent hydraulic roughness predicted by this modified GM model, $z_{oa} = 2.04$ cm, is in better agreement with the measured value of 2.78 cm than the 1.26 cm afforded by the standard GM model. Apparent hydraulic roughness estimates predicted in this manner for all experiments are presented in Table 1 (under the heading "Predicted $z_{oa}$, cm, $\delta$ Set at 6 cm") and show that the use of an enhanced boundary layer thickness improves the agreement between predicted and measured apparent hydraulic roughness for all experiments. However, the predicted $z_{oa}$ values obtained from the modified GM model still underestimate the actual $z_{oa}$ values, as is evident in Figure 3 where the predicted curve still falls below the data. Thus even after modification of the wave boundary layer thickness, a significant discrepancy still exists between predicted and measured velocity profiles.

## 5. Effects of Wave-Induced Mass Transport

### GM Model With Wave-Induced Mass Transport

To resolve the discrepancy between observed and predicted velocity profiles for wave-current boundary layers, a reanalysis of the application of the Grant-Madsen model to these experiments is necessary. The Grant-Madsen model is based on a time-invariant eddy viscosity. However, turbulence characteristics in combined wave-current boundary layers will have some time variation. *Trowbridge and Madsen* [1984b] showed that a time-varying eddy viscosity significantly affects the nature of steady mass transport for pure second-order Stokes' waves.

A time-varying eddy viscosity can effect a mass transport component for combined wave-current flows as well. Following *Trowbridge and Madsen* [1984a, b], the shear stress $\tau$ in the wave boundary layer flow may be represented by

$$\tau/\rho = \nu_t(\partial u/\partial z) \tag{5}$$

where $\rho$ is the fluid density and $\nu_t$ is a time-varying eddy viscosity. For second-order Stokes' waves the horizontal velocity may be represented by a steady component $u_c$, a first harmonic time-varying component $u_1$, and a second harmonic time-varying component $u_2$, such that

$$u = u_c + u_1 + u_2 \tag{6}$$

Since the horizontal bottom orbital velocity has an asymmetric time variation, the near-bottom turbulence characteristics will exhibit a first harmonic as well as a second harmonic time variation. Therefore the eddy viscosity may be separated into steady, first harmonic, and second harmonic components, such that

$$\nu_t = \nu_c + \nu_1 + \nu_2 \tag{7}$$

By substituting (6) and (7) into (5) and time averaging, an equation governing the time-averaged shear stress can be written as

$$\nu_c \frac{\partial u_c}{\partial z} = \frac{\bar{\tau}}{\rho} - \overline{\nu_1 \frac{\partial u_1}{\partial z}} - \overline{\nu_2 \frac{\partial u_2}{\partial z}} \tag{8}$$

The steady current in this equation is driven by three terms: a time-averaged shear stress term and two eddy viscosity interaction terms. The time-averaged shear stress term includes a time-averaged shear stress associated with the current ($\tau_c$) and a time-averaged shear stress arising from dissipation of wave energy within the wave boundary layer ($\bar{\tau}_w$). The first eddy viscosity interaction term represents interactions between the first harmonic component of the eddy viscosity and the first harmonic velocity gradient, and the second eddy viscosity term represents interactions between the second harmonic component of the eddy viscosity and second harmonic velocity gradient. In the GM model a time-invariant eddy viscosity is used such that the two eddy viscosity interaction terms drop out of

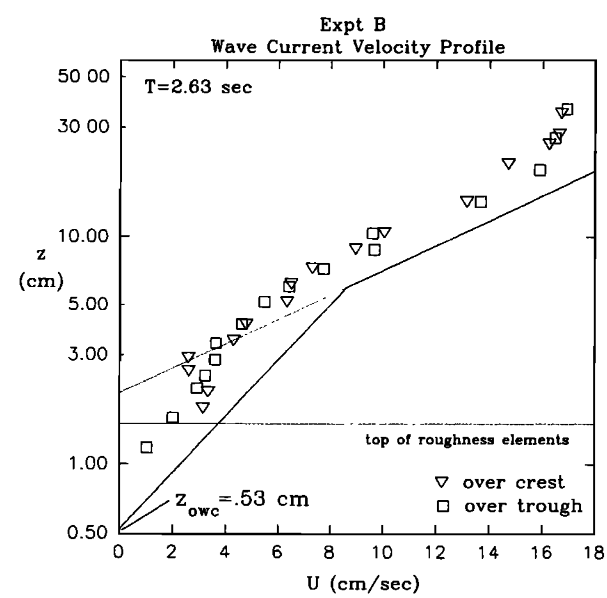


**Figure 3.** Time-averaged velocity profile for combined wave-current flow ($U$ = 16 cm/s and $T$ = 2.63 s): comparison with velocity profile predicted by GM model (modified for $\delta$ = 6 cm).

(8) and the wave attenuation is neglected such that the steady velocity (in this case, the current) is solely driven by the current shear stress $\tau_c$.

As noted above, *Trowbridge and Madsen* [1984a, b] used a time-varying eddy viscosity model to show that the two interaction terms contribute to the mass transport for pure Stokes' waves (with no current present). A time-varying eddy viscosity was also included in a linear wave-current model developed by *Madsen and Wikramanayake* [1991]. Since the magnitude of $\nu_1$ in this case is related to the magnitude of the current shear stress, which generally is much smaller than the wave-associated shear stress, *Madsen and Wikramanayake* [1991] concluded that the term $\overline{\nu_1 \partial u_1/\partial z}$ would have an insignificant effect on the mean velocity profile. This observation suggests that any wave-induced mass transport for Stokes' waves in the presence of a current is dominated by wave effects and therefore is approximately equal to that obtained for waves alone. In this case the wave-induced mass transport for a combined wave-current flow would be the same as for a pure progressive wave and a solution to (8) may be written

$$u = u_c + \bar{u}_w \quad (9)$$

In this equation, $u_c$ is given by the Grant-Madsen model and represents the velocity associated with the current shear stress, while $\bar{u}_w$ is the mass transport velocity exclusively associated with the wave motion.

In principle, the mass transport represented by $\bar{u}_w$ is equivalent to the wave-induced mass transport predicted by the time-varying eddy viscosity model of *Trowbridge and Madsen* [1984a, b] (TM). However, the TM model relies on the detailed velocity structure inside the wave boundary layer for its prediction of the steady wave-induced mass transport. Just as the GM model fails to predict wave velocities inside the wave boundary layer for the large roughness values encountered here, so will the TM model fail in its prediction of $\bar{u}_w$. Estimates of $\bar{u}_w$ must therefore be obtained experimentally.

### Wave-Induced Mass Transport for Pure Waves

Time-averaged velocity profiles were measured for pure waves in order to estimate the wave-induced mass transport denoted as $\bar{u}_w$. The time-averaged velocity profiles measured over the crest and trough for the pure wave experiment corresponding to wave-current experiment B (in Table 1) are shown in Figure 4. For elevations above 20 cm the average velocity is approximately −1.0 cm/s. As the elevation decreases from 20 to 6 cm, the average velocity decreases from −1.0 to −1.2 cm/s. The region from 0 to 6 cm may be defined as the wave boundary layer. Spatial bottom variability associated with the ripples has a significant effect on the time-averaged velocity profile for most of the wave boundary layer, which, as noted earlier, has a larger thickness than predicted by the GM model. The time-averaged velocity is negative (−1.2 cm) at the edge of the enhanced wave boundary layer, in qualitative agreement with the prediction of the TM model.

The nonlinear nature of Stokes' waves imposes a steady mass transport in the flume which must be balanced by a steady return current to satisfy continuity. For experiment b this calculated theoretical return current is −1.1 cm/s, which closely matches the −1.0 cm/s velocity above 20 cm shown in Figure 4. This Eulerian return current interacts with the apparent bottom roughness to form a current boundary layer which develops in space with distance from its leading edge (e.g., from the toe of the absorber beach). Because of this boundary layer development, the magnitude of the return current velocity should be extremely small relative to the wave-induced mass transport at the edge of the wave boundary layer. Thus the wave-induced mass transport velocity observed at the edge of the wave boundary layer is the streaming generated from processes within the wave boundary layer.

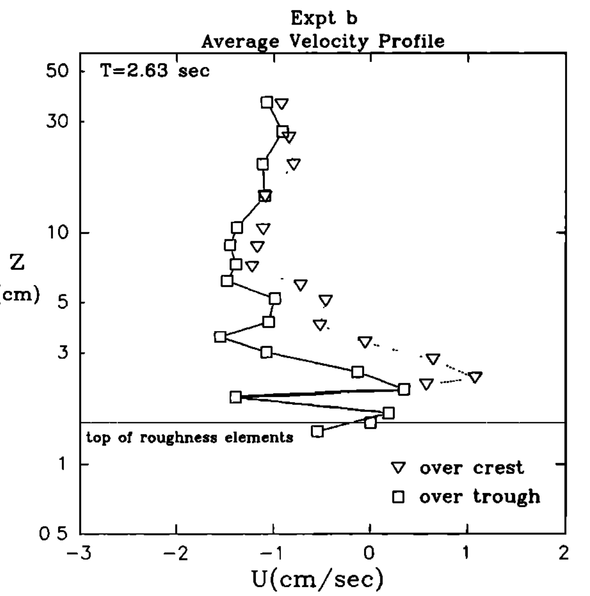


**Figure 4.** Time-averaged velocity profile for pure waves ($T$ = 2.63 s).

To verify this assertion, an additional experiment was completed in which the pump was used to generate an extremely low current velocity to match and therefore eliminate the Eulerian return current. The proper flow rate was set by first conducting an experimental run over a flat bed and using velocity measurements to ensure that the return current was essentially eliminated. Then, with the rippled bed, one experiment was completed with the current set to balance the return current and another with no current generation such that a return current existed in the flume. Time-averaged velocity profiles were measured over crest and trough for both runs. As shown in Figure 5, the mean velocities measured at the edge of the wave boundary layer were essentially the same for both runs. Therefore at the edge of the wave boundary layer the magnitude of the return current is negligible, and the measured time-averaged velocity provides an accurate estimate of the wave-induced streaming. At $z$ = 30 cm the return velocity without pumping (≈−1.4 cm/s) is stronger than the return velocity with pumping (≈−0.7 cm/s) reflecting the approximate removal of the return current by pumping. Table 1 includes estimates of wave-induced streaming, $\bar{u}_w$, at the edge of the enhanced wave boundary layer ($\delta$ = 6 cm) for all pure wave experiments completed.

### Effects of Wave-Induced Streaming on Currents in the Presence of Waves

Since the wave conditions for pure wave experiments and wave-current experiments were chosen to be virtually the same, the pure wave mass transport estimates provide estimates for wave-induced streaming in combined wave-current experiments. The velocity at the edge of the wave boundary layer serves as a bottom boundary condition for the current

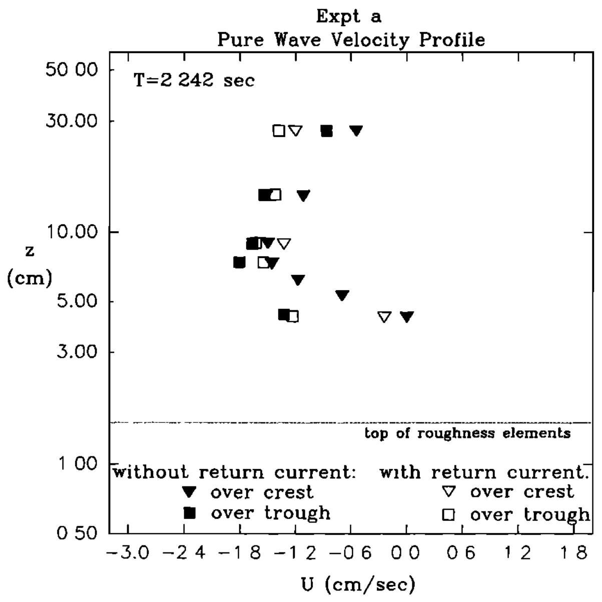


**Figure 5.** Time-averaged velocity profile for pure waves compared with profile obtained if pump is used to remove return current.

velocity profile in the upper region outside of the wave boundary layer. Therefore the entire time-averaged velocity profile outside of the wave boundary layer may be translated by an amount equal to the pure wave-induced mass transport at the edge of the wave boundary layer. For elevations above the wave boundary layer the modified velocity profile is defined by (9) where $u_c$ is the time-averaged velocity profile predicted by the GM model including the effect of enhanced wave boundary layer thickness (i.e., $\delta$ = 6 cm) and $\bar{u}_w$ is the wave-induced mass transport at the edge of the wave boundary layer.

The modified velocity profile for experiment B is shown in Figure 6. As noted in Table 1, the pure wave-induced streaming for experiment b was −1.2 cm/s. For the region of the velocity profile which is above 6 cm the modified profile is obtained by translating the former velocity profile (shown in Figure 3) to the left by 1.2 cm/s. Thus the solid line in Figure 6 shows the predicted velocity profile when wave-induced mass transport is accounted for. The dashed line in Figure 6 is simply a straight line drawn so that a continuous velocity profile is defined between $z_{owc}$ and $\delta$. As noted previously, due to the large bottom roughness, the wave-induced mass transport within the wave boundary layer cannot be predicted. As can be seen in Figure 6, accounting for the wave-induced mass transport improves the fit to the data outside of the wave boundary layer considerably and leads to an apparent hydraulic roughness $z_{oa}$ = 2.37 cm in excellent agreement with the observed 2.78 cm.

As shown above, for all wave-current experiments, predicted current profiles were determined using the GM model modified for the enhanced boundary layer thickness and accounting for wave-induced streaming. These predicted apparent roughnesses are listed in Table 1 under the heading "Predicted $z_{oa}$, cm, With Mass Transport and $\delta$ = 6 cm." For every experiment, accounting for wave-induced mass transport resulted in a closer correspondence between measured and predicted apparent hydraulic roughnesses than the match afforded by the GM model with the modified wave boundary layer thickness. This improvement indicates that wave-induced mass transport should be accounted for to accurately predict the apparent roughness experienced by a current in a combined wave-current flow.

## Current Roughness in the Presence of Waves

In the preceding section, estimates of the wave roughness in the presence of a current, $k_{wc}$, were used as input to the modified GM model to determine an apparent hydraulic roughness $z_{oa}$. Another approach is to use the measured values of the apparent roughness, current shear velocity, and measured wave-induced mass transport as inputs to the modified GM model to estimate the equivalent Nikuradse bottom roughness. This latter analysis is greatly facilitated by introducing a modified apparent hydraulic roughness $z'_{oa}$, defined by

$$z'_{oa} = z_{oa} \exp\left(\kappa \overline{u_w}/u_{*c}\right) \tag{10}$$

By introducing (10) into (1), it is readily shown that this choice for $z'_{oa}$ produces the desired translation of the GM model by an amount of $-\bar{u}_w$; that is, $z'_{oa}$ represents an apparent hydraulic roughness which would exist if the effects of wave-induced streaming were eliminated. A value for the hydraulic roughness for the current in the presence of waves, $z_{ocw}$, is then obtained from (2) if $z_{oa}$ is replaced by $z'_{oa}$ and $\delta$ = 6 cm is used for $\delta_{wc}$. Finally, a bottom roughness estimate that represents the bottom roughness experienced by the current in the presence of waves is obtained from $k_{cw} = 30 z_{ocw}$.

The $k_{cw}$ estimates, along with the roughness results of MM1, are summarized in Table 2. Review of the data in Table 2 indicates that more variability is apparent in the $k_{cw}$ values than in the $k_{wc}$ or $k_w$ values. The somewhat larger variability in $k_{cw}$ measurements may be due to variability of the second harmonic wave components. Interactions at the second harmonic frequency are primarily responsible for the first harmonic forcing term $\overline{\nu_1 \partial u_1/\partial z}$ in (9), which governs the wave-induced mass transport. Although wave generation was modified to effectively remove the second free harmonic from

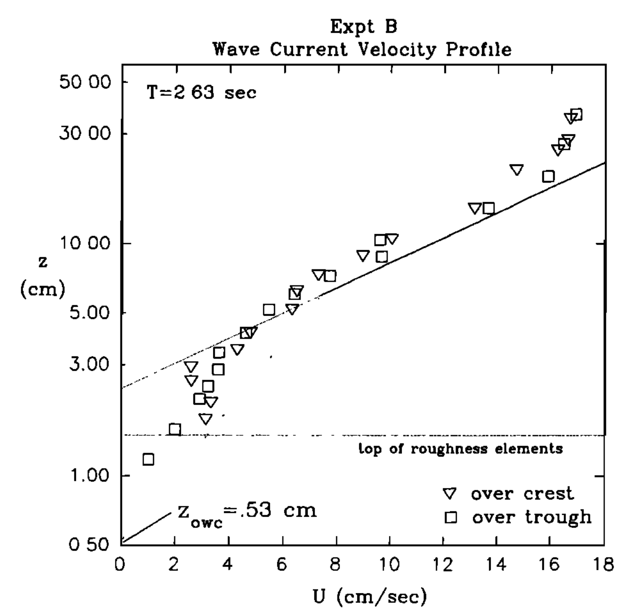


**Figure 6.** Time-averaged velocity profile for combined wave-current flow ($U$ = 16 cm/s and $T$ = 2.63 s): comparison with velocity profile predicted by GM model (modified for wave-induced mass transport and $\delta$ = 6 cm).

**Table 2.** Roughness Comparisons

| Experiment ID | $T$, s | $U$, cm/s | $A_b$, cm | $k_{cw}$, cm | $k_{wc}$, cm | $k_w$, cm | $k_c$, cm |
|---|---|---|---|---|---|---|---|
| A | 2.24 | 16 | 6.45 | 29.6 | 19.5 | 28.0 | 23.6 |
| B | 2.63 | 16 | 8.08 | 22.5 | 15.7 | 22.3 | 23.6 |
| C | 2.89 | 16 | 8.80 | 23.0 | 17.7 | 17.6 | 23.6 |
| G | 2.24 | 12 | 6.37 | ··· | 20.1 | 28.0 | 18.1 |
| H | 2.63 | 12 | 8.00 | 12.6 | 15.0 | 22.3 | 18.1 |
| I | 2.89 | 12 | 8.84 | ··· | 24.9 | 17.6 | 18.1 |
| J | 2.24 | 12 | 4.31 | 26.7 | 21.3 | 25.6 | 18.1 |
| K | 2.63 | 12 | 5.61 | 13.4 | 18.4 | 25.5 | 18.1 |
| L | 2.89 | 12 | 6.12 | 45.9 | 23.0 | 23.6 | 18.1 |
| M* | 2.24 | 16 | 6.61 | ··· | 11.5 | 8.6 | ··· |
| N* | 2.63 | 16 | 8.22 | 28.3 | 10.7 | 8.6 | ··· |
| O* | 2.89 | 16 | 9.11 | ··· | 12.5 | 6.2 | ··· |
| P* | 2.24 | 12 | 6.55 | ··· | 9.6 | 8.6 | 12.6 |
| O* | 2.63 | 12 | 8.20 | 15.2 | 12.2 | 8.6 | 12.6 |
| R* | 2.89 | 12 | 9.18 | ··· | 16.2 | 6.2 | 12.6 |

*Twenty-centimeter roughness spacing.

the flume, free second harmonics could not be completely eliminated. These minor free harmonic components could have some effect on the wave-induced streaming. In addition, wave-induced mass transport for the combined wave-current conditions was estimated from measurements in pure wave experiments. Some variability could be a result of minor differences between the second harmonic components for pure waves and waves in the presence of a current.

Roughness determinations for currents in the presence of waves ($k_{cw}$), waves in the presence of a current ($k_{wc}$), pure waves ($k_w$), and pure currents ($k_c$) can be compared using arithmetic averages of roughness estimates listed in the four columns of Table 2. For the 10-cm roughness spacing the arithmetic average value of the bottom roughness experienced by the current in the presence of waves ($k_{cw}$) is 24.8 cm, which is in general agreement with the arithmetic average values of 19.6 cm for waves in the presence of currents ($k_{wc}$), 23.8 cm for pure waves ($k_w$), and 20.9 cm for pure currents ($k_c$). For 20-cm spacing experiments the roughness for the current in the presence of waves is somewhat larger than other roughness estimates for this spacing. However, since only two $k_{cw}$ values were obtained for the 20-cm spacing, roughness comparisons for 20-cm spacing are considered to be inconclusive and are not considered further.

Since the roughness enters (1) as a factor in the argument of the logarithmic function, it is appropriate to represent the roughness in terms of a geometric mean rather than an arithmetic mean [*Madsen et al.*, 1993]. Comparing roughnesses for the 10-cm spacing in terms of a geometric mean yields mean values of 22.8 cm for $k_{cw}$, 19.3 cm for $k_{wc}$, 23.5 cm for $k_w$, and 20.7 cm for $k_c$. On the basis of these four roughness estimates, a mean roughness is determined to be 21.4 cm. Each of the four roughness estimates is within 10% of this mean roughness, indicating an accuracy of 10%, which is significantly more accurate than our present ability to predict the bottom roughness for a movable sediment bed. For practical purposes the $k_{cw}$ estimates are therefore equal to the $k_{wc}$, $k_w$, and $k_c$ values; that is, the roughness experienced by a current in the presence of waves is the same as the roughnesses for pure currents, pure waves, and waves in the presence of a current.

## 6. Summary and Discussion

The experimental results summarized in this paper and its companion paper (MM1) show that a single roughness can be used to characterize pure currents, pure waves, and both waves and currents in combined wave-current flows. Since all results were analyzed using the *Grant and Madsen* [1986] eddy viscosity model, this conclusion is predicated on application of this model. However, while application of the wave-current theory of *Grant and Madsen* [1986] showed the pure current roughness ($k_c$) and wave roughnesses ($k_w$ and $k_{wc}$) to be the same, the theory could not successfully predict the current velocity profiles in the presence of waves. For all experiments the GM model greatly underestimated the apparent hydraulic roughness experienced by the current, $z_{oa}$. This discrepancy was partially attributed to the large roughness elements which were necessary to simulate a rippled bed similar to bed forms in the previous movable bed experiments of *Mathisen* [1989] and *Rosengaus* [1987]. Boundary layers for the experiments were enhanced due to these large roughness elements and did not correspond to the prediction of the GM model. By modifying the GM model to include this enhanced boundary layer thickness, the discrepancy between observed and predicted velocity profiles was reduced.

The remaining discrepancy between predicted and measured velocity profiles was attributed to the influence of wave-induced mass transport within the wave boundary layer. A conceptual model was presented ((8) and (9)), in which the horizontal velocity is comprised of the velocity predicted by the GM model modified to account for an enhanced wave boundary layer thickness ($u_c$) and a streaming or mass transport at the edge of the wave boundary layer strictly associated with the wave motion ($\bar{u}_w$).

In principle, this wave-induced mass transport is theoretically equivalent to the wave-induced streaming predicted by the eddy viscosity model of *Trowbridge and Madsen* [1984a, b]. However, mass transport predictions obtained using the *Trowbridge and Madsen* [1984a, b] model did not match the experimental measurements. Predictions of the *Trowbridge and Madsen* [1984a, b] model do not match the data because the model is only valid for relative roughnesses, $A_b/k_w$, greater than 10, while the relative roughnesses for these experiments were less than 1. The model's predictions, however, were in qualitative agreement with experimental observations of a mass transport at the outer edge of the wave boundary layer in the direction opposite that of wave propagation.

Since the *Trowbridge and Madsen* [1984a, b] model could not be used to estimate $\bar{u}_w$ for these experiments, estimates for $\bar{u}_w$ were obtained from velocity profiles measured during experiments with waves alone. An additional experiment was completed which showed that the effects of return currents were negligible at the edge of the wave boundary layer. Consequently, velocities measured at the edge of the wave boundary layer were solely attributed to wave-induced mass transport. Since the wave conditions for the pure wave experiments were essentially the same as for the combined wave-current experiments, these wave-induced streaming measurements could be used to estimate $\bar{u}_w$ for the combined wave-current flow experiments.

Thus the measurements obtained at the edge of the wave boundary layer were used to determine the effects of wave-induced transport on the velocity profile for the region outside of the wave boundary layer. Accounting for the effects of wave-induced streaming in combined wave-current velocity profiles resolved the discrepancy between predicted and measured current velocity profiles. Therefore, by accounting for this wave-induced streaming, a single bottom roughness length scale was shown to characterize the effects of the bottom for pure current, pure wave, and combined wave-current boundary layer flows.

Although the results of the present experimental investigation verified the single roughness assumption universally made in theoretical models of turbulent wave-current bottom boundary layer flows, some qualifying remarks are in order. The above conclusion was reached only for codirectional wave-current flows and only after the *Grant and Madsen* [1986] model was modified to account for (1) an enhanced boundary layer thickness and (2) the presence of a wave-induced streaming at the outer edge of the wave boundary layer. It is believed that both of these modifications would be required of any existing theoretical model for combined wave-current boundary layer flows if it were to provide predictions in reasonable agreement with the experimental results presented here. Yet there exists, to the authors' knowledge, no adequate theory for large bottom roughnesses which could be applied for the prediction of the necessary modifications which were determined experimentally here. The present investigation's verification of the existence of a single bottom roughness scale is therefore not the end but a call for further studies of combined wave-current boundary layer flows over rippled beds.

**Acknowledgments.** The research presented in this paper was sponsored by the MIT Sea Grant College Program under grant NA90-AA-D-SG424 from the Office of Sea Grant, National Oceanic and Atmospheric Administration, U.S. Department of Commerce, and represents the doctoral dissertation of Paul P. Mathisen, prepared under the guidance of Ole S. Madsen at Ralph M. Parsons Laboratory, Massachusetts Institute of Technology. The authors acknowledge the insightful comments of anonymous reviewers and especially express appreciation for the contributions of one extremely meticulous review.

## References

Bakker, W. T. T., and T. van Doorn, Near-bottom velocities in waves with a current, in *Proceedings of the 16th International Conference on Coastal Engineering*, pp. 1394–1413, Am. Soc. of Civ. Eng., New York, 1978.

Brevik, I., and B. Aas, Flume experiment on waves and currents, I, Rippled bed, *Coastal Eng.*, *3*, 149–177, 1980.

Christoffersen, J. B., and I. C. Jonsson, Bed friction and dissipation in a combined current and wave motion, *Ocean Eng.*, *12*(5), 387–423, 1985.

Grant, W. D., and O. S. Madsen, Combined wave and current interaction with a rough bottom, *J. Geophys. Res.*, *84*(C4), 1797–1808, 1979.

Grant, W. D., and O. S. Madsen, The continental shelf boundary layer, *Annu. Rev. Fluid Mech.*, *18*, 265–305, 1986.

Kemp, P. H., and R. R. Simons, The interaction of waves and a turbulent current: Waves propagating with the current, *J. Fluid Mech.*, *116*, 227–250, 1982.

Lundgren, H., Turbulent currents in the presence of waves, in *Proceedings of the 13th International Conference on Coastal Engineering*, pp. 623–634, Am. Soc. of Civ. Eng., New York, 1972.

Madsen, O. S., and P. N. Wikramanayake, Simple models for turbulent wave-current bottom boundary layer flow, Final report for the Dredging Research Program, *Contract Rep. DRP-91-1*, U.S. Army Corps of Eng., Coastal Eng. Res. Cent., Vicksburg, Miss., 1991.

Madsen, O. S., L. D. Wright, J. D. Boon, and T. A. Chisholm, Wind stress, bed roughness, and sediment suspension on the inner shelf during an extreme storm event, *Cont. Shelf Res.*, *13*(11), 1303–1324, 1993.

Mathisen, P., Experimental study on the response of fine sediments to wave agitation and associated wave attenuation, M.S. thesis, Mass. Inst. of Technol., Cambridge, 1989.

Mathisen, P., Bottom roughness for wave and current boundary layer flows over a rippled bed, Ph.D. thesis, Mass. Inst. of Technol., Cambridge, 1993.

Mathisen, P., and O. S. Madsen, Bottom roughness for waves and current boundary layer flows over a rippled bed, *Sea Grant Rep. MITSG 93-27*, Sea Grant College Program, Mass. Inst. of Technol., Cambridge, 1993.

Mathisen, P., and O. S. Madsen, Waves and currents over a fixed rippled bed, 1, Bottom roughness experienced by waves in the presence and absence of currents, *J. Geophys. Res.*, this issue.

Rosengaus, M., Experimental study on wave generated bedforms and resulting wave attenuation, Ph.D. thesis, Mass. Inst. of Technol., Cambridge, 1987.

Smith, J. D., Modeling of sediment transport on continental shelves, in *The Sea*, vol. 6, *Marine Modelling*, edited by E. D. Goldberg et al., pp. 538–577, John Wiley, New York, 1977.

Tanaka, H., and N. Shuto, Friction coefficient for a wave-current coexisting system, *Coastal Eng. Jpn.*, *24*, 105–128, 1981.

Trowbridge, J., and O. S. Madsen, Turbulent wave boundary layers, 1, Model formulation and first-order solution, *J. Geophys. Res.*, *89*(C5), 7989–7997, 1984a.

Trowbridge, J., and O. S. Madsen, Turbulent wave boundary layers, 1, Second-order theory and mass transport, *J. Geophys. Res.*, *89*(C5), 7999–8007, 1984b.

O. S. Madsen, Ralph M. Parsons Laboratory, Department of Civil and Environmental Engineering, Massachusetts Institute of Technology, Cambridge, MA 02139.

P. P. Mathisen, Department of Civil and Environmental Engineering, Worcester Polytechnical Institute, 100 Institute Road, Worcester, MA 01609. (e-mail: mathisen@wpi.edu)

(Received November 15, 1994; revised July 5, 1995;
accepted November 20, 1995.)